TL1A inhibits atherosclerosis in apoE-deficient mice by regulating the phenotype of vascular smooth muscle cells

Received for publication, August 4, 2020, and in revised form, September 1, 2020 Published, Papers in Press, September 22, 2020, DOI 10.1074/jbc.RA120.015486

Dan Zhao[1,2], Jiaqi Li[1], Chao Xue[1], Ke Feng[1], Lipei Liu[1], Peng Zeng[1], Xiaolin Wang[1], Yuanli Chen[1], Luyuan Li[3], Zhisong Zhang[3], Yajun Duan[2], Jihong Han[1,*], and Xiaoxiao Yang[2,*]

From the [1]College of Life Sciences, Key Laboratory of Bioactive Materials of Ministry of Education, State Key Laboratory of Medicinal Chemical Biology, Nankai University, Tianjin, China, the [2]Key Laboratory of Metabolism and Regulation for Major Diseases of Anhui Higher Education Institutes, College of Food and Biological Engineering, Hefei University of Technology, Hefei, China, and the [3]College of Pharmacy, Nankai University, Tianjin, China

Edited by Dennis R. Voelker

TNF ligand-related molecule 1A (TL1A) is a vascular endothelial growth inhibitor to reduce neovascularization. Lack of apoE a expression results in hypercholesterolemia and atherosclerosis. In this study, we determined the precise effects of TL1A on the development of atherosclerosis and the underlying mechanisms in apoE-deficient mice. After 12 weeks of pro-atherogenic high-fat diet feeding and TL1A treatment, mouse aorta, serum, and liver samples were collected and used to assess atherosclerotic lesions, fatty liver, and expression of related molecules. We found that TL1A treatment significantly reduced lesions and enhanced plaque stability. Mechanistically, TL1A inhibited formation of foam cells derived from vascular smooth muscle cells (VSMCs) but not macrophages by activating expression of ABC transporter A1 (ABCA1), ABCG1, and cholesterol efflux in a liver X receptor–dependent manner. TL1A reduced the transformation of VSMCs from contractile phenotype into synthetic phenotypes by activating expression of contractile marker α smooth muscle actin and inhibiting expression of synthetic marker osteopontin, or osteoblast-like phenotype by reducing calcification. In addition, TL1A ameliorated high-fat diet–induced lipid metabolic disorders in the liver. Taken together, our work shows that TL1A can inhibit the development of atherosclerosis by regulating VSMC/foam cell formation and switch of VSMC phenotypes and suggests further investigation of its potential for atherosclerosis treatment.

Atherosclerosis is one of the common causes of cardiovascular diseases, which can seriously impair human health. It is also a complex pathophysiological process, characterized by disorders of cholesterol/lipid metabolism, inflammation, and ultimately the development of fibrous plaques in the aorta (1, 2). Previous studies have demonstrated that monocyte/macrophage accumulation and infiltration, endothelial cell dysfunctions, and vascular smooth muscle cell (VSMC) phenotypic differentiation play important roles in the development of atherosclerosis (3, 4).

Physiologically, VSMCs are contractile differentiated cells with a low ability of proliferation and apoptosis within the middle layer of vessel wall (5). The primary functions of VSMCs are to regulate the vessel tone as well as blood pressure and flow distribution (6). However, during the development of atherogenesis, VSMCs can switch from a contractile phenotype to a synthetic phenotype, associated with increased expression of synthetic markers, such as osteopontin (OPN), and reduced expression of contractile markers, such as α smooth muscle actin (αSMA) and smooth muscle protein 22α (SM22α) (7). VSMCs can also differentiate into osteoblast-like cells that drives the process of calcification. Vascular calcification increases plaque vulnerability and exacerbates atherosclerosis progression (8). In addition, excess lipids accumulating in VSMCs can promote foam cell formation and contribute to the total intimal foam cell population in lesions (9). In fact, VSMCs contribute the majority of foam cells in both human coronary atherosclerosis and advanced mouse atherosclerosis (10, 11). Moreover, VSMC/foam cells are potentially detrimental to plaque stability (12).

TNF ligand–related molecule 1A (TL1A), also known as vascular endothelial growth inhibitor or tumor necrosis factor superfamily 15, is a type II transmembrane protein. It can be produced predominantly by endothelial cells in response to inflammatory cytokines (13, 14). In addition to regulation of neovascularization, high levels of TL1A were detected in human carotid atherosclerotic plaques, especially in macrophage/foam cells (15). Furthermore, TL1A and its receptor, the death domain–containing receptor 3, participate in formation of human macrophage/foam cells by increasing uptake of oxidized low-density lipoprotein (oxLDL) and reducing cholesterol efflux *in vitro* (16). Therefore, TL1A may be a mediator of atherosclerosis. However, whether TL1A can affect atherosclerosis *in vivo* remains unknown.

Although apoE-deficient (apoE$^{-/-}$) mice can spontaneously develop atherosclerotic lesions when they are fed chow diet, the pro-atherogenic high-fat diet (HFD)-fed apoE$^{-/-}$ mice have been used more frequently as the model for atherosclerosis investigation. Compared with chow diet, HFD feeding can substantially reduce the time for development of lesions. In addition, the HFD feeding can generate severe human-like hypercholesterolemia in the animals (17, 18). Therefore, in this study, we used HFD-fed apoE$^{-/-}$ mice to determine the effect of TL1A on the development of atherosclerosis and the involved mechanisms.

This article contains supporting information.

* For correspondence: Jihong Han, jihonhan2008@nankai.edu.cn; Xiaoxiao Yang, xiaoxiaoyang@hfut.edu.cn.

Results

TL1A inhibits atherosclerosis in apoE$^{-/-}$ mice

To determine whether TL1A can influence the development of atherosclerosis, we fed apoE$^{-/-}$ mice the pro-atherogenic HFD for 12 weeks, a duration that can induce lesions substantially. Meanwhile, mice were intraperitoneally (i.p.) injected with PBS (control group) or recombinant human TL1A protein (TL1A group), twice a week. At the end of treatment, we collected aortic samples and determined both *en face* arterial and aortic root sinus lesions by Oil Red O staining. Compared with lesions in control mice ($\sim 8.9 \times 10^6$ μm^2), TL1A treatment reduced *en face* aortic lesions to $\sim 4.7 \times 10^6$ μm^2 (Fig. 1*A*, *left* and *middle panels*). Meanwhile, in different segments of aortas (Fig. 1*B*), TL1A treatment inhibited the progression of lesions in descending aorta, thoracic aorta, and abdominal aorta, but not aortic arch (Fig. 1*A*, *right panel*). Furthermore, TL1A treatment substantially reduced sinus lesion size in aortic root, from 6.04×10^5 in the control group to 4.43×10^5 μm^2 in the TL1A-treated group (Fig. 1*C*).

To investigate the effect of TL1A on vascular structure, we determined collagen content and necrotic areas in aortic root cross-sections. Fig. 1*D* shows that TL1A substantially reduced the area of necrotic cores (~50%) while increasing thickness of the fibrous caps (~1.5-fold) and collagen content (~1.5-fold) in lesion areas, indicating that TL1A enhances plaque stability.

Vascular calcification can increase risk of vulnerable lesion rupture (19). By completing the Alizarin Red S staining of aortic root cross-sections, we found a marked decrease of calcification-positive areas in lesion areas of TL1A-treated mice (Fig. 1*E*). Taken together, these results suggest that TL1A inhibits the development of atherosclerosis, enhances lesion stability, and reduces vascular calcification.

To assess whether the inhibition of lesions by TL1A is related to changes of serum lipid profiles, levels of total, low-density lipoprotein (LDL)-, and high-density lipoprotein (HDL)-cholesterol and triglyceride were determined. As shown in Table 1, TL1A had little effect on lipid profiles, suggesting that the reduction of atherosclerosis is unrelated to serum cholesterol levels.

TL1A promotes formation of macrophage/foam cells

Although macrophage/foam cells play an important role in atherosclerosis, our results show that TL1A had little effect on monocyte/macrophage marker 2 (MOMA2) levels in aortic root (Fig. 2*A*). In addition, more foam cells were determined with peritoneal macrophages collected from TL1A-treated mice than controls (Fig. 2*B*), which is consistent with the previous report that TL1A stimulates differentiation of foam cells from either THP-1/PMA macrophages or primary human monocyte-derived macrophages *in vitro* (16).

To further confirm the effects of TL1A on formation of macrophage/foam cells, we isolated peritoneal macrophages from C57BL/6J mice and treated the oxLDL-loaded cells with TL1A or TL1A plus T0901317 (T317, a synthetic ligand for liver X receptor (LXR), can inhibit formation of macrophage/foam cells). As shown in Fig. 2*C*, TL1A moderately increased the number of foam cells both in the presence or absence of oxLDL, whereas the number was reduced by T317 in the presence of oxLDL. Meanwhile, TL1A antagonized T317-reduced foam cells. Both ABC transporter A1 (ABCA1) and ABCG1, two target genes of LXR, are the main molecules mediating macrophage cholesterol efflux to reduce foam cell formation and activated by T317 (17). At the molecular level, TL1A alone had moderate effects on ABCA1 expression but inhibited ABCG1 expression. In addition, TL1A substantially attenuated T317-induced ABCA1/G1 expression (Fig. 2, *D* and *E*).

CD36 is a classic receptor for uptake of oxLDL by monocyte/macrophages, thereby facilitating formation of macrophage/foam cells and atherosclerosis development. CD36 can be activated by the transcription factor of peroxisome proliferator-activated receptor γ (PPARγ) (20), whereas sterol-responsive nuclear receptors, LXRα and LXRβ, are key determinants of cellular cholesterol homeostasis and promote cellular cholesterol efflux by up-regulating ABCA1 and ABCG1 expression (21). We found that although TL1A alone moderately induced expression of PPARγ and its target, CD36, in macrophages, it did not further enhance the oxLDL-induced PPARγ and CD36 levels (Fig. 2, *F* and *G*). In contrast, LXRα and LXRβ expression was decreased by TL1A treatment in the presence or absence of oxLDL (Fig. 2, *F* and *G*). Functionally, we found that TL1A reduced cholesterol efflux to HDL from macrophages (Fig. 2*H*). Taken together, these results suggest that TL1A promotes formation of foam cells derived from macrophages by inducing CD36 expression and inhibiting ABCA1/G1 expression. It also implies that TL1A-inhibited atherosclerosis is unrelated to the formation of macrophage/foam cells.

TL1A enhances plaque stability by regulating VSMC phenotypic changes and reducing formation of VSMC/foam cells

VSMC is another main cell type making contributions to atherosclerosis by various mechanisms. For instance, the cell phenotypic switch of VSMCs plays a vital role in plaque stability (9). To determine the effect of TL1A on VSMC phenotypic changes, we completed immunofluorescent staining of aortic root cross-sections with anti-αSMA and -OPN antibody. We found that expression of αSMA, the contractile marker linking to collagen content, was obviously elevated, whereas expression of OPN, the synthetic phenotype marker, was significantly reduced in TL1A-treated mice (Fig. 3*A*). These data indicate that TL1A can regulate the number of VSMCs in different phenotypes.

We further defined the role of TL1A in VSMC phenotypic changes *in vitro* by treating human primary aortic smooth muscle cells (HASMCs) with TL1A. At the mRNA levels, we found that TL1A increased levels of the contractile phenotype markers, such as αSMA and SM22α, while reducing levels of OPN and epiregulin (EREG), two proliferative markers (Fig. 3*B*, *left half*). Serum response factor (SRF) and myocardin (Myocd) can form SRF-Myocd complex, and the complex functions as major transcription factors to maintain high αSMA expression and VSMCs as a contractile phenotype. The SRF-Myocd complex can be negatively regulated by Msh homeobox 1 or 2 (Msx1/2) (22). We determined that TL1A induced expression

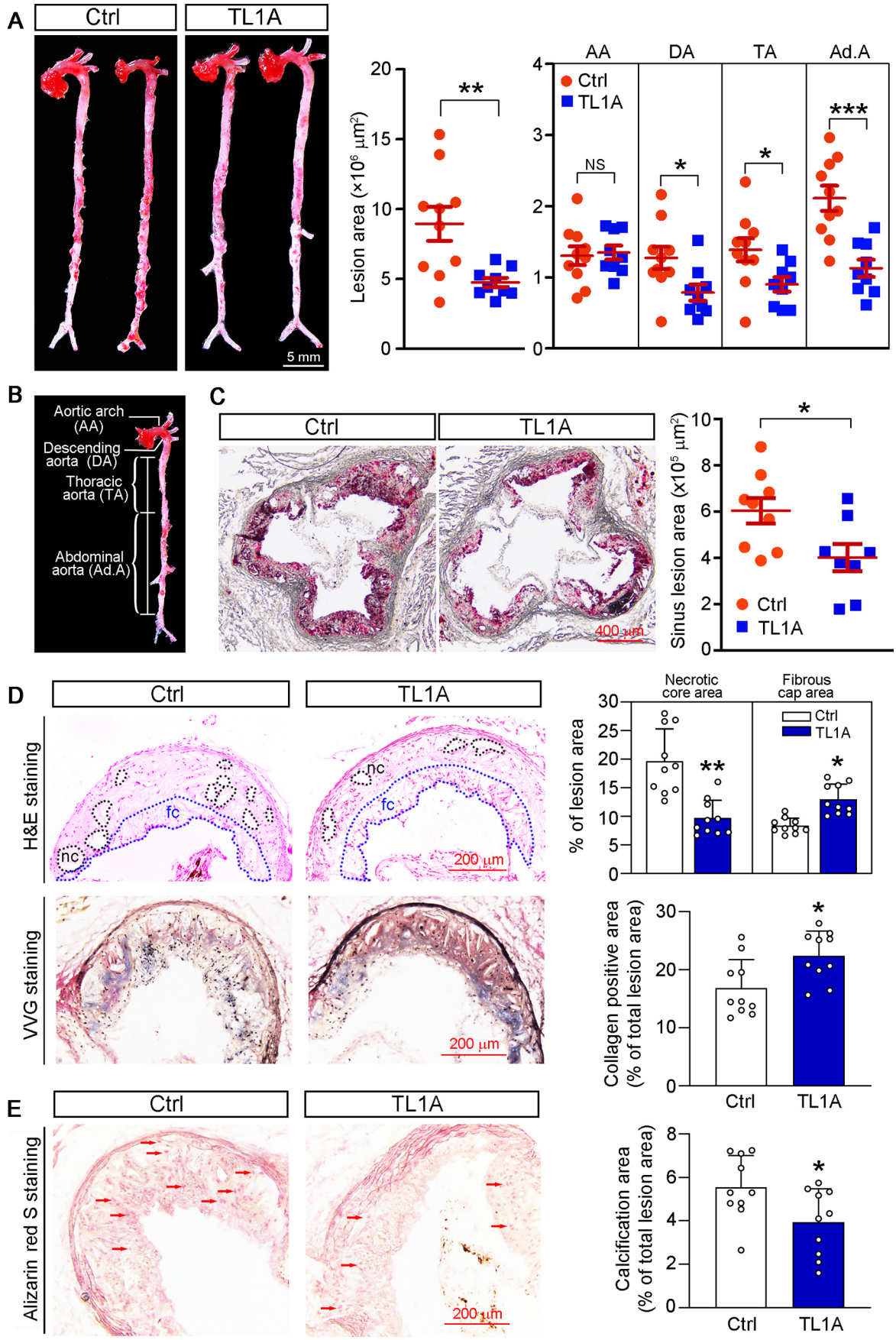
A
Ctrl
TL1A
5 mm
Lesion area (×10⁶ μm²)
**
AA
DA
TA
Ad.A
Ctrl
TL1A
NS
*
*
***
B
Aortic arch (AA)
Descending aorta (DA)
Thoracic aorta (TA)
Abdominal aorta (Ad.A)
C
Ctrl
TL1A
400 μm
Sinus lesion area (x10⁵ μm²)
*
Ctrl
TL1A
D
Ctrl
TL1A
H&E staining
nc
fc
200 μm
VVG staining
200 μm
Necrotic core area
Fibrous cap area
% of lesion area
**
*
Collagen positive area (% of total lesion area)
*
Ctrl
TL1A
E
Ctrl
TL1A
Alizarin red S staining
200 μm
Calcification area (% of total lesion area)
*
Ctrl
TL1A

Table 1

TL1A treatment has little effect on serum lipid profiles and body weight gain. Male apoE$^{-/-}$ mice (~8 weeks old) were randomly divided into two groups (10 mice/group) and received the treatment indicated in Fig. 1. At the end of the experiment, levels of serum total, LDL- and HDL-cholesterol and triglyceride were determined

Parameter	Control	TL1A
Total cholesterol (mM)	35.724 ± 3.669	36.03 ± 4.629
LDL-cholesterol (mM)	12.645 ± 1.436	12.925 ± 1.359
HDL-cholesterol (mM)	5.175 ± 0.578	5.771 ± 0.959
Triglyceride (mM)	0.942 ± 0.069	1.092 ± 0.187
Body weight (g)	32.73 ± 2.051	32.34 ± 2.327
Liver weight/body weight (%)	6.103 ± 0.388	6.111 ± 0.914

of SRF and Myocd and correspondingly reduced Msx2 expression (Fig. 3*B*, *right half*).

Several studies indicate that microRNAs (miRNAs) play an important role in regulating VSMC phenotype transformation. For example, up-regulation of miR-214 by hypoxia mediates VSMC phenotypic modulation and proliferation (23). miR-145, one of the most abundant VSMC miRNAs, mitigates a phenotypic switch from the contractile state into the proliferative one by inducing Myocd expression (24). miR-29b mimics reduces cell viability and promotes SMC apoptosis by inhibiting expression of matrix metalloproteinase 2 (MMP2), one of the MMPs that enhances the VSMC switch from the contractile phenotype into the synthetic phenotype (25, 26). In this study, we found that TL1A decreased miR-214-5p expression but increased expression of miR-145 and miR-29b (Fig. 3*C*, *left three panels*). Therefore, changes of the VSMC cell population in different phenotypes by TL1A are also related to the effect of TL1A on expression of the aforementioned miRNAs.

Accumulating studies indicate that tumor suppressor p53 overexpression promotes SMC from the synthetic phenotype of migration characteristics to the quiescent and contractile phenotype by activating Myocd (27). We determined that TL1A significantly induced p53 expression in a dose-dependent manner, which was associated with decreased OPN and increased αSMA and SM22α expression proportionally (Fig. 3*D*). Reciprocally, when p53 expression in HASMCs was reduced by transfecting with p53 siRNA, expression of αSMA and SM22α was also markedly decreased, whereas the effect of TL1A on expression of these molecules was substantially attenuated (Fig. 3*E*). Taken together, the data above suggest that TL1A is able to regulate the VSMC cell population in different phenotypes and appears to enhance the switch of VSMCs from the synthetic/proliferative phenotype into the contractile phenotype by regulating expression of p53 and related miRNAs.

However, the switch of VSMC phenotypes can be completed by different mechanisms. Enhancement of the apoptosis of VSMCs in the synthetic phenotype can also generate the apparent VSMC phenotype switch, particularly in the context of TL1A enhancing expression of p53 and miR-29b, two molecules that may enhance cell apoptosis. To determine the role of TL1A on cell apoptosis *in vivo*, we conducted TUNEL staining of the cross-sections of aortic root and thoracic aorta and quantified the number of TUNEL-positive cells. As shown in Fig. S1, TL1A had little effect on the number of apoptotic cells. Meanwhile, TL1A had little effect on expression of apoptosis-related genes, such as caspase-3, B cell lymphoma 2 (BCL2), and BCL2-associated X protein (BAX) in lesion areas either (Fig. S2). Consistent with *in vivo* results, we found that TL1A did not affect the viability of peritoneal macrophages (Fig. S3*A*) and HASMCs cultured either in normal medium or calcification medium (Fig. S3, *B* and *C*) (calcification medium can restrain cell growth; therefore, reduced cell viability was observed compared with cells cultured in normal medium). Furthermore, expression of apoptotis-related proteins was not altered by TL1A either (Fig. S3, *D–G*). Therefore, the results above suggest that the switch of VSMC phenotypes is not tightly linked to cell apoptosis.

Similar to macrophages, VSMCs in synthetic phenotype are prone to differentiate into foam cells during atherosclerosis, and foam cells derived from VSMCs also potently contribute to the development of atherosclerosis (11). Thus, we investigated the effects of TL1A on VSMC/foam cell formation. HASMCs were treated with TL1A or TL1A plus oxLDL, followed by Oil Red O staining. Loading oxLDL to HASMCs potently increased Oil Red O–positive cells. However, TL1A clearly reduced HASMC/foam cells (Fig. 4*A*). Mechanistically, we determined that expression of ABCA1 and ABCG1 was increased, particularly in the presence of oxLDL. Similar to macrophages, TL1A increased CD36 and PPARγ expression in HASMCs. However, TL1A inhibited oxLDL-activated CD36 and PPARγ expression (Fig. 4, *B–E*). In contrast to macrophages, TL1A alone activated LXRα and LXRβ expression and further enhanced oxLDL-induced LXR expression (Fig. 4, *D* and *E*). Correspondingly, TL1A activated ABCA1 and ABCG1 expression in HASMCs and enhanced cholesterol efflux from HASMCs (Fig. 4, *B*, *C*, and *F*). *In vivo*, TL1A treatment substantially enhanced ABCG1 with little effect on ABCA1 expression (Fig. 4*G*). Taken together, the results above demonstrate that TL1A treatment reduces formation of foam cells derived from VSMCs mainly by enhancing ABCA1/G1 expression with LXRα/β activation and promoting cholesterol efflux.

TL1A inhibits vascular calcification by inhibiting osteoblast differentiation

The results of Verhoeff–Van Gieson (VVG) and Alizarin Red S staining (Fig. 1, *D* and *E*) demonstrate that TL1A can enhance plaque stability, which is related to reduction of vascular

Figure 1. Recombinant TL1A inhibits atherosclerosis in apoE$^{-/-}$ mice. *A* and *B*, after 12 weeks treatment, aortas were collected and conducted Oil Red O staining to determine *en face* aortic lesions. Representative images are presented (*left panel*), and *en face* aortic lesion areas or lesion areas in aortic arch (*AA*), descending aorta (*DA*), thoracic aorta (*TA*), and abdominal aorta (*Ad.A*) were quantitatively analyzed (*right panels*). *C*, the aortic root cross-sections were prepared, and Oil Red O staining was conducted to determine sinus lesion areas. Representative images are presented (*left*) with quantitative analysis of lesion areas (*right*). *D*, H&E and VVG staining of aortic root cross-sections (*left panels*) with quantitative analysis of necrotic core (*nc*), fibrous cap (*fc*), and collagen content (*right panels*). *E*, calcification in sinus lesion area was determined by Alizarin Red S staining. Representative images are presented with quantitation of calcification-positive area. *Red arrows*, calcium deposition in the arterial wall. *, $p < 0.05$; **, $p < 0.01$; ***, $p < 0.001$ *versus* control group; *NS*, not significantly different (*A*, $n = 10$ for Ctrl, 9 for TL1A; *C*, $n = 9$ for Ctrl, 8 for TL1A; *D* and *E*, $n = 10$ for both Ctrl and TL1A). *Error bars*, S.D.

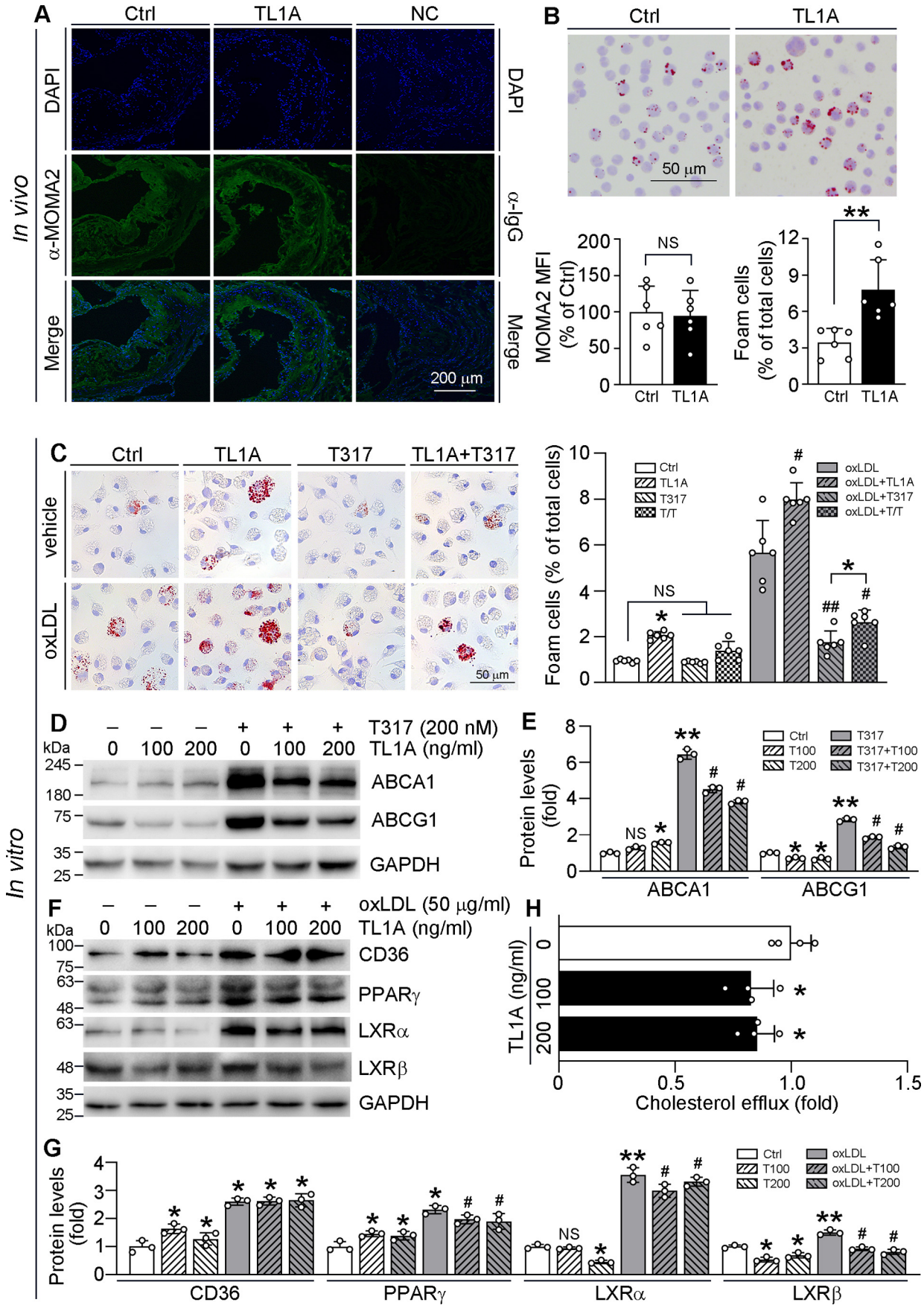
A
Ctrl
TL1A
NC
In vivo
DAPI
α-MOMA2
Merge
α-IgG
200 μm
B
Ctrl
TL1A
50 μm
MOMA2 MFI (% of Ctrl)
NS
Foam cells (% of total cells)
**
C
Ctrl
TL1A
T317
TL1A+T317
vehicle
oxLDL
50 μm
Foam cells (% of total cells)
Ctrl
TL1A
T317
T/T
oxLDL
oxLDL+TL1A
oxLDL+T317
oxLDL+T/T
NS
In vitro
D
T317 (200 nM)
TL1A (ng/ml)
kDa
245
180
75
35
25
ABCA1
ABCG1
GAPDH
E
Protein levels (fold)
Ctrl
T100
T200
T317
T317+T100
T317+T200
ABCA1
ABCG1
F
oxLDL (50 μg/ml)
TL1A (ng/ml)
kDa
100
75
63
48
63
48
35
25
CD36
PPARγ
LXRα
LXRβ
GAPDH
H
TL1A (ng/ml)
Cholesterol efflux (fold)
G
Protein levels (fold)
CD36
PPARγ
LXRα
LXRβ
oxLDL
oxLDL+T100
oxLDL+T200

calcification. To further define the functions of TL1A on vascular calcification, we conducted immunofluorescence staining to determine the expression of runt-related transcription factor 2 (RUNX2), a key transcriptional factor in osteogenic differentiation, and its downstream genes, alkaline phosphatase (ALP) and MMP9. As shown in Fig. 5 (*A* and *B*), expression of RUNX2, ALP, and MMP9 was reduced by TL1A, which was associated with reduced RUNX2 nuclear translocation.

Vascular calcification is widely acknowledged as a potent risk factor for plaque rupture and the consequent sudden cardiovascular events (28). The osteoblast-like cells deriving from VSMCs in calcified plaques plays an important role in the process of vascular calcification (29). Therefore, we further determined the effects of TL1A on HASMC calcification *in vitro*. The results of Alizarin Red S staining in Fig. 5*C* show that calcification medium caused severe calcium accumulation within cells. However, the accumulation was clearly attenuated by TL1A. The quantification of cellular calcium content further confirms the inhibitory effect of TL1A on calcification (Fig. 5*D*).

In addition, the results of immunofluorescent staining and Western blotting demonstrate that calcification medium induced RUNX2 expression and nuclear translocation in HASMCs, which was reduced by TL1A (Fig. 5, *E–G*). Consequently, calcification medium–activated expression of other critical molecules for osteoblast differentiation, such as bone morphogenetic protein 2 (BMP2), ALP, and OPN proteins in HASMCs, was reduced by TL1A (Fig. 5, *H* and *I*). Associated with changes in protein levels, mRNA levels of these osteogenic phenotype markers increased by calcification medium were attenuated by TL1A (Fig. 5*J*). To further confirm the direct effect of TL1A on RUNX2 activity, we constructed a RUNX2 promoter (*p*RUNX2). As shown in Fig. 5 (*K* and *L*), TL1A decreased calcification medium–activated RUNX2 promoter activity.

It has been reported that miR-203-3p can suppress osteoblast differentiation by targeting RUNX2 (30). Interestingly, we found that treatment of HASMCs with TL1A increased miR-203-3p expression (Fig. 3*C*, *right*), another underlying mechanism for inhibition of VSMC osteogenic differentiation by TL1A. Taken together, the results above demonstrate that TL1A inhibits vascular calcification by inactivating RUNX2 pathway both *in vivo* and *in vitro*.

Discussion

Chronic inflammation is a key factor in atherogenesis. It destroys the arterial wall microenvironment and contributes to plaque formation (1). Previous study has revealed that TL1A, as an important cytokine, plays a pathological role in different inflammatory diseases, such as rheumatoid arthritis, inflammatory bowel disease, and asthma, by mediating inflammatory reactions (31). In this study, we demonstrated that apoE$^{-/-}$ mice treated with TL1A showed a significant decrease of plaque areas, especially in descending aorta, thoracic aorta, and abdominal aorta (Fig. 1, *A* and *C*). Furthermore, we demonstrated that TL1A enhanced plaque stability and inhibited calcification (Fig. 1, *D* and *E*). However, TL1A treatment had little effect on food intake and body weight gain in mice. It also had no effect on other parameters, such as liver weight and serum lipid profiles (Table 1).

Compared with apoE$^{-/-}$ mice receiving PBS injection, no visible damage areas in the liver were determined by hematoxylin and eosin (H&E) staining after TL1A treatment (Fig. S4*A*). Meanwhile, the levels of serum aspartate aminotransferase (AST), alanine aminotransferase (ALT), and ALP were not changed (Fig. S4*B*), indicating the high safety with the long-term TL1A administration.

We previously reported that amelioration of hepatic lipid metabolism is a positive effect of anti-atherosclerosis (32, 33). In this study, although TL1A has little effect on hypercholesterolemia in HFD-fed apoE$^{-/-}$ mice, it reduced TG accumulation in the liver (Fig. S4, *C* and *D*). Mechanistically, we determined that expression of hormone-sensitive lipase (HSL) and adipose triglyceride lipase (ATGL) protein was increased by TL1A (Fig. S4, *E* and *F*). Consistently, co-activator comparative gene identification-58 (CGI-58), HSL, and ATGL mRNA levels were also elevated (Fig. S4*G*). However, TL1A had little effect on acyl-CoA:diacylglycerol acyltransferase 1 (DGAT1) expression (Fig. S4, *E–G*). The effect of TL1A on hepatic DGAT1, HSL, and ATGL was further confirmed by immunohistochemical staining (Fig. S4*H*). TL1A treatment substantially increased phosphorylated AMP-activated protein kinase α (*p-AMPKα*) (Fig. S4, *E* and *F*), a master regulator for cellular energy homeostasis, by inducing HSL and ATGL and inhibiting DGAT1 expression (34). We further observed that TL1A significantly decreased acetyl-CoA levels in the liver (Fig. S5*A*), indicating that TL1A promotes fatty acid oxidation. Acetyl-CoA carboxylase, an enzyme involved in lipid metabolism, along with its phosphorylated form, was increased by TL1A. Meanwhile, TL1A treatment up-regulated fatty acid oxidation–related genes, PPARα, carnitine palmitoyltransferase 1A (CPT1A), and acyl-CoA oxidase 1 (ACOX1), at protein and mRNA levels in both mouse liver and HepG2 cells (Fig. S5, *B–G*). Taken together, these results indicate that the reduction of hepatic lipid accumulation by TL1A can be attributed to activation of TG hydrolysis and fatty acid oxidation.

Figure 2. TL1A enhances differentiation of macrophage/foam cells by inhibiting ABCA1 and ABCG1 expression. *A*, aortic cross-sections of mice used in Fig. 1 were subjected to immunofluorescent staining with anti-MOMA2 antibody, and the mean fluorescent intensity (MFI) in images was quantitatively analyzed. *NS*, not significantly different ($n = 6$). *NC*: negative control. *B*, peritoneal macrophages collected from mice used in Fig. 1 were subjected to Oil Red O staining to assess formation of foam cells (>10 lipid droplets/cell). **, $p < 0.01$ ($n = 6$). *C*, peritoneal macrophages isolated from C57BL/6J mice in serum-free medium were treated with TL1A (200 ng/ml), T0901317 (T317; 200 nM), or TL1A plus T317 (*T/T*) for 24 h. Cells were then incubated with oxLDL (50 μg/ml) for 4 h, followed by Oil Red O staining and quantification of foam cells. *, $p < 0.05$ *versus* control or as indicated; #, $p < 0.05$; ##, $p < 0.01$ *versus* oxLDL-treated alone; *NS*, not significantly different ($n = 6$). *D–G*, peritoneal macrophages were treated with TL1A, T317, oxLDL (50 μg/ml), TL1A plus T317, or oxLDL at the indicated concentrations for 24 h. Expression of ABCA1, ABCG1, CD36, PPARγ, LXRα, and LXRβ protein was determined by Western blotting with quantitative analysis of band density. *, $p < 0.05$; **, $p < 0.01$ *versus* control; #, $p < 0.05$ *versus* T317 or oxLDL-treated alone; *NS*, not significantly different ($n = 3$). *H*, macrophages were prelabeled with [^{3}H]cholesterol for 24 h. Cells were then treated with TL1A at the indicated concentrations for 24 h, followed by determination of cholesterol efflux to HDL. *, $p < 0.05$ *versus* control ($n = 4$). *Error bars*, S.D.

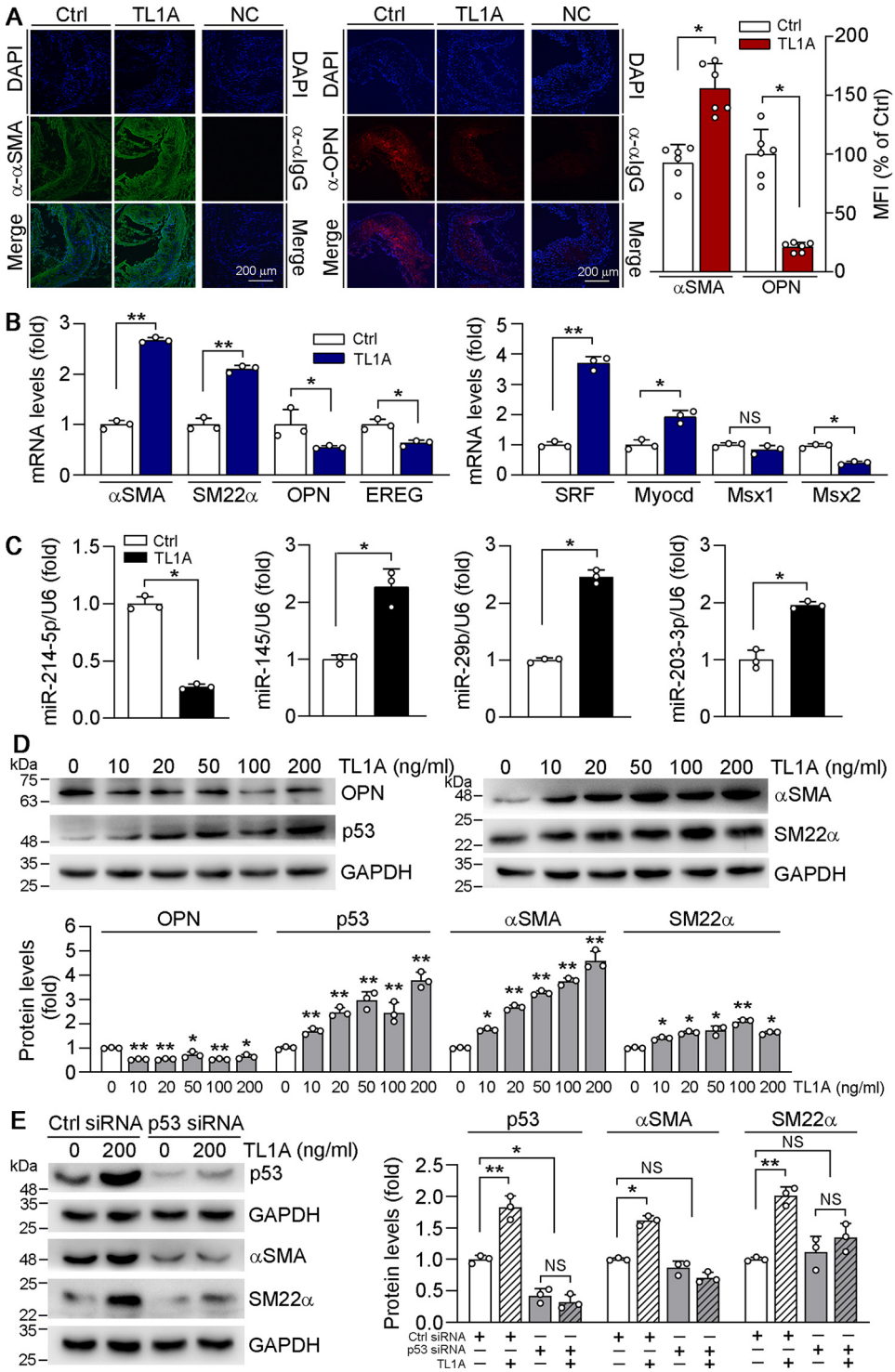

Figure 3. TL1A inhibits VSMC phenotypic switch by regulating expression of miRNAs, OPN, p53, αSMA, and SM22α. *A*, aortic root cross-sections were subjected to immunofluorescent staining with anti-αSMA and OPN antibody, and MFI in images was quantified. The *NC* in the *right panel* (for OPN) was conducted with an adjacent slide to the *NC* slide in Fig. 5*A*. *, $p < 0.05$ ($n = 6$). *B–D*, HASMCs were treated with TL1A (200 ng/ml) for 24 h. Expression of αSMA, SM22α, OPN, EREG, SRF, Myocd, Msx1, and Msx2 mRNA (*B*) and miR-214-5p, miR-145, miR-29b, and miR-203-3p was determined by qRT-PCR (*C*). Expression of OPN, p53, αSMA, and SM22α protein was determined by Western blotting with quantitative analysis of band density (*D*). *E*, HASMCs were transfected with scrambled (*Ctrl*) or p53 siRNA for 24 h and then treated with TL1A (200 ng/ml) for 24 h. Expression of p53, αSMA, and SM22α protein was determined by Western blotting with quantitative analysis of band density. *, $p < 0.05$; **, $p < 0.01$ *versus* control or as indicated; *NS*, not significantly different ($n = 3$). *Error bars*, S.D.

Classically, the intimal VSMCs plays a pivotal role in the formation of fibrous cap of lesions, which can stabilize atherosclerotic plaques (19). Under normal circumstances, VSMCs exhibit a low proliferation rate and mainly express contractile proteins, such as αSMA and SM22α. However, many studies demonstrate that VSMCs are not terminally differentiated and

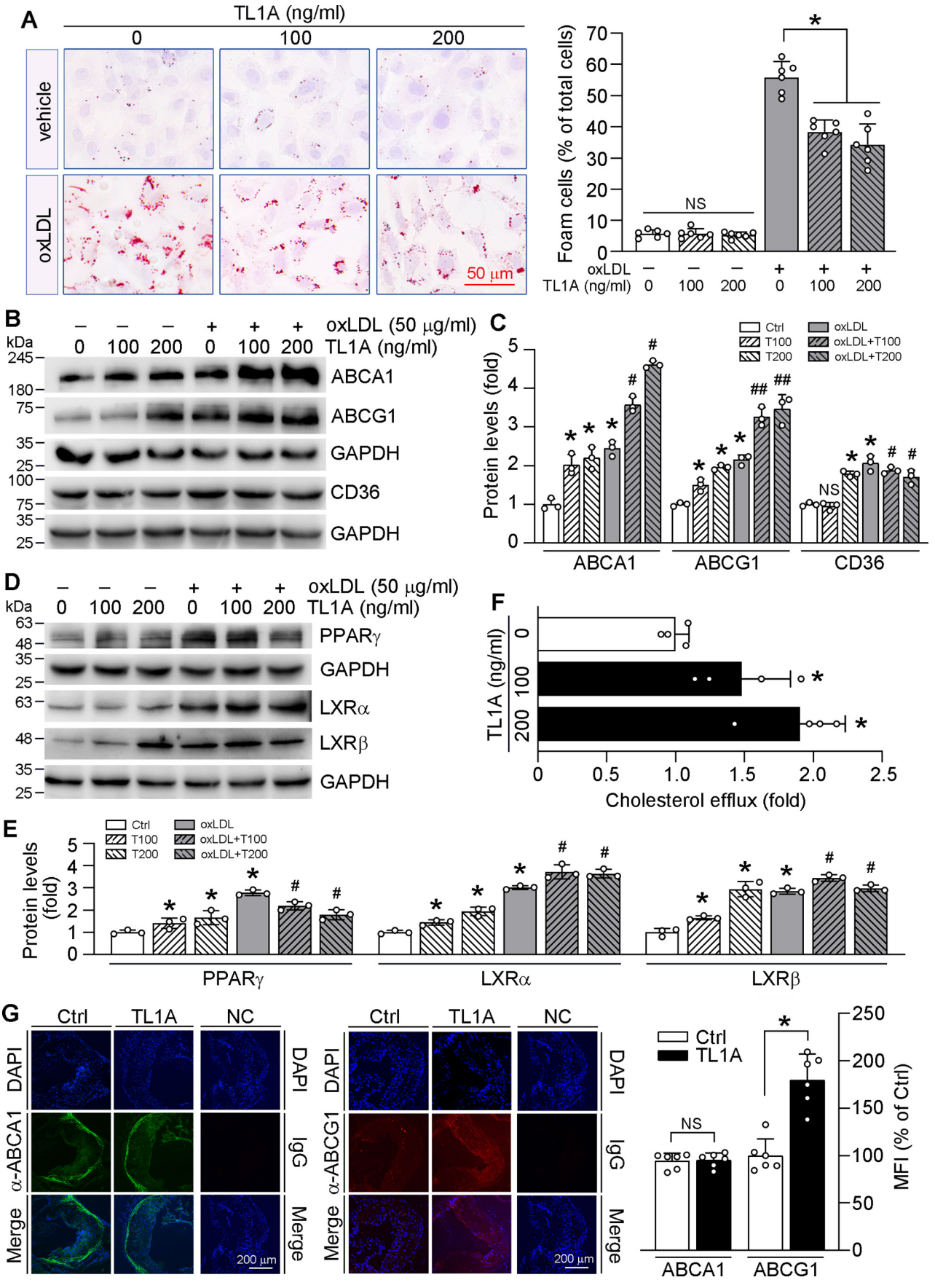
A
TL1A (ng/ml)
0
100
200
vehicle
oxLDL
50 μm
Foam cells (% of total cells)
NS
oxLDL
TL1A (ng/ml)
B
oxLDL (50 μg/ml)
TL1A (ng/ml)
kDa
ABCA1
ABCG1
GAPDH
CD36
GAPDH
C
Ctrl
T100
T200
oxLDL
oxLDL+T100
oxLDL+T200
Protein levels (fold)
ABCA1
ABCG1
CD36
D
PPARγ
GAPDH
LXRα
LXRβ
GAPDH
E
PPARγ
LXRα
LXRβ
F
TL1A (ng/ml)
Cholesterol efflux (fold)
G
Ctrl
TL1A
NC
DAPI
α-ABCA1
α-ABCG1
IgG
Merge
200 μm
MFI (% of Ctrl)

can migrate into intima during the initiation of atherosclerotic plaques, where VSMCs undergo a phenotypic switch with high expression of synthetic markers, such as OPN (35). VSMCs transformed into the synthetic phenotype will lose the contractile property, which is potentially detrimental to plaque stability. Our results show that TL1A enhances plaque stability by regulating expression of genes involved in the VSMC phenotype switch from the synthetic phenotype into the contractile phenotype (Fig. 3, *A* and *B*).

It is commonly believed that p53 is implicated in cell apoptosis. Numerous studies have well-demonstrated the influence of p53 on atherosclerosis, which is completed in an apoptosis-independent manner. For instance, deficiency of p53 expression in apoE$^{-/-}$ mice accelerates aortic atherosclerosis by increasing cell proliferation rate, not apoptosis (36). In our previous study, we demonstrated that inhibition of vascular calcification by DNA topoisomerase II inhibitors is related to activation of p53 expression (37). However, we observed that DNA topoisomerase II inhibitors have no effect on proliferation and apoptosis of HASMCs (27). In current study, we also observed that regulation of VSMC phenotype transformation by TL1A is associated with activation of p53 expression (Fig. 3, *D* and *E*), whereas TL1A had no effect on cell apoptosis in aortas or macrophages/HASMCs (Figs. S1 and S3 (*A–C*)). Therefore, although we demonstrated that p53 is a critical mediator for the TL1A-regulated VSMC phenotype switch, the regulation is not tightly linked to apoptosis of VSMCs in synthetic phenotype. In addition, TL1A treatment significantly reduced vascular calcification both *in vivo* and *in vitro* (Figs. 1*E* and 5*C*), which is associated with regulation of osteoblast differentiation–related gene expression by regulating the RUNX2 pathway (Fig. 5, *A*, *B*, *E–L*).

Switch from contractile to synthetic phenotype can expedite the lipid accumulation in VSMCs (7). Formation of lipid-laden VSMC/foam cells in the arterial wall is another major hallmark of atherosclerosis and tightly linked to plaque instability (7). In this study, we found TL1A substantially suppressed formation of oxLDL-induced VSMC/foam cells *in vitro* (Fig. 4*A*), mainly by activating expression of ABCA1 and ABCG1 and cholesterol efflux through LXR activation (Fig. 4, *B–F*).

The previous study reports that TL1A can accelerate formation of macrophage/foam cells *in vitro* (16). In fact, formation of cholesterol-rich macrophage/foam cells mainly occurs at the early stage of atherosclerotic lesions, whereas the advanced lesions are characterized by accumulation of VSMC/foam cells (9, 38). Recently, it has been demonstrated that VSMCs contribute the majority of foam cells in both human coronary atherosclerosis and established mouse atherosclerosis (35, 38). Similarly, we determined that TL1A enhanced formation of macrophage/foam cells while having little effect on macrophage/foam cells in lesion areas (Fig. 2). However, TL1A inhibited VSMC phenotypic switch from contractile phenotype into synthetic phenotype and/or osteoblast phenotype and activated ABCA1/G1 expression, thereby ultimately and potently impeding formation of VSMC/foam cells and enhancing plaque stability. It also suggests that inhibition of atherosclerosis by TL1A mainly depends on its actions on VSMCs (Fig. S6).

Experimental procedures

Materials

TL1A recombinant protein was kindly provided by Dr. Luyuan Li (Nankai University). Rabbit anti-ABCA1 (catalog no. NB400-105) polyclonal antibody was purchased from Novus Biologicals (Littleton, CO). Rabbit anti-ABCG1 (catalog no. 13578-1-AP), CD36 (catalog no. 18836-1-AP), PPARγ (catalog no. 16643-1-AP), LXRα (catalog no. 14351-1-AP), ALP (catalog no. 11187-AP), BMP2 (catalog no. 18933-1-AP), Lamin A/C (catalog no. 10298-1-AP), and OPN (catalog no. 22952-1-AP) polyclonal antibodies and mouse anti-LXRβ (catalog no. 60345-1-Ig) polyclonal antibody were purchased from Proteintech Group Inc. (Chicago, IL, USA). Rabbit anti-MMP9 (catalog no. A2095) polyclonal antibody was purchased from ABclonal Technology (Wuhan, Hubei, China). Mouse anti-αSMA (catalog no. sc-130617) mAb and rat anti-MOMA2 (catalog no. sc-59332) mAb were purchased from Santa Cruz Biotechnology, Inc. (Dallas, TX, USA). Rabbit anti-RUNX2 (catalog no. AF5186) polyclonal antibody was purchased from Affinity (Cincinnati, OH, USA). TRIzol reagent was purchased from Invitrogen. The reverse transcription kit was purchased from Promega (Madison, WI, USA). SYBR Green Master Mix was purchased from Bio-Rad. Goat anti-rabbit IgG (whole molecule)-FITC (catalog no. F0382) was purchased from Sigma–Aldrich. Rhodamine phalloidin was purchased from Yeason (Shanghai, China). All other reagents were purchased from Sigma–Aldrich.

Animals and study design

The protocols for animal studies were approved by the Committee of the Ethics of Experimental Animals at Nankai University. All of the *in vivo* studies were conformed to the Guide for the Care and Use of Laboratory Animals published by National Institutes of Health (NIH publication 85-23, revised in 1985).

Male apoE$^{-/-}$ mice (~8 weeks old) were bought from the Animal Center of Nanjing University (Nanjing, China). The apoE$^{-/-}$ mice were randomly divided into two groups (10 mice/group): the control group and the TL1A group. Mice were fed a pro-atherogenic HFD (21% fat plus 0.5% cholesterol) for 12 weeks. During the HFD feeding, mice in TL1A group

Figure 4. TL1A inhibits formation of VSMC/foam cells by enhancing expression of ABCA1 and ABCG1. *A–E*, HASMCs were treated with TL1A at the indicated concentrations, oxLDL (50 μg/ml), or TL1A plus oxLDL as indicated for 48 h. Oil Red O staining was conducted to assess formation of HASMC/foam cells (>10 lipid droplets/cell) (*A*). *, $p < 0.05$; *NS*, not significantly different ($n = 6$). Expression of ABCA1, ABCG1, CD36, PPARγ, LXRα, and LXRβ protein was determined by Western blotting with quantitative analysis of band density (*B–E*). *, $p < 0.05$ *versus* control; #, $p < 0.05$; ##, $p < 0.01$ *versus* oxLDL-treated alone; *NS*, not significantly different ($n = 3$). *F*, HASMCs were prelabeled with [^{3}H]cholesterol for 24 h, and cells were then treated with TL1A at the indicated concentrations for 24 h, followed by determination of cholesterol efflux to HDL. *, $p < 0.05$ *versus* control ($n = 4$). *G*, expression of ABCA1 and ABCG1 in aortic root cross-sections was determined by immunofluorescent staining with quantitative analysis of MFI. The *NC* for *left* and *right panels* was conducted with two adjacent slides. *, $p < 0.05$; *NS*, not significantly different ($n = 6$). *Error bars*, S.D.

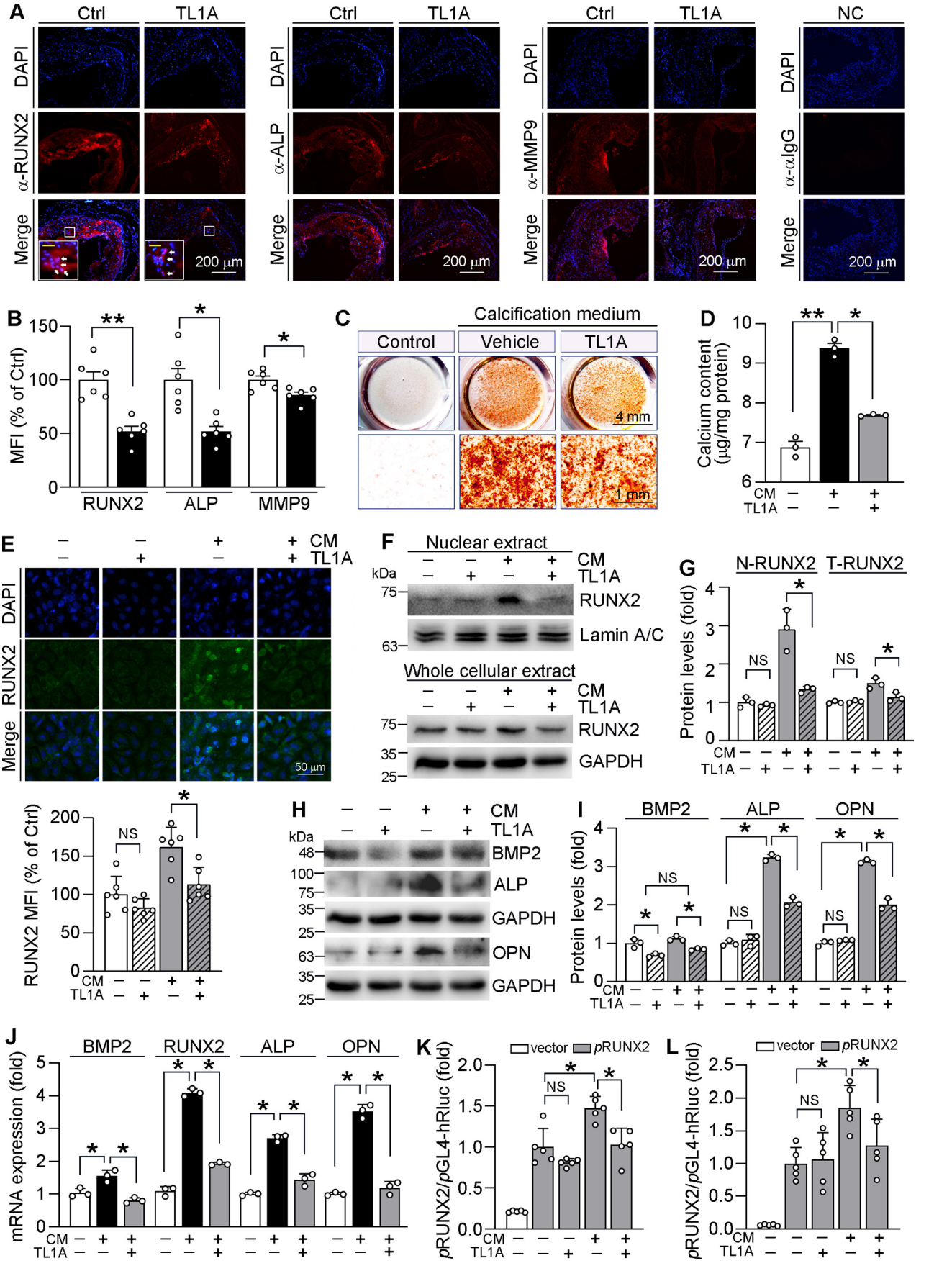
A
Ctrl
TL1A
NC
DAPI
α-RUNX2
α-ALP
α-MMP9
α-IgG
Merge
200 μm
B
MFI (% of Ctrl)
RUNX2
ALP
MMP9
C
Calcification medium
Control
Vehicle
TL1A
4 mm
1 mm
D
Calcium content (μg/mg protein)
CM
TL1A
E
CM
TL1A
DAPI
RUNX2
Merge
50 μm
RUNX2 MFI (% of Ctrl)
NS
F
Nuclear extract
Whole cellular extract
kDa
RUNX2
Lamin A/C
GAPDH
G
N-RUNX2
T-RUNX2
Protein levels (fold)
H
BMP2
ALP
OPN
I
BMP2
ALP
OPN
Protein levels (fold)
J
mRNA expression (fold)
BMP2
RUNX2
ALP
OPN
K
vector
pRUNX2
pRUNX2/pGL4-hRluc (fold)
L
vector
pRUNX2
pRUNX2/pGL4-hRluc (fold)

were i.p. injected with 0.5 ml of recombinant TL1A solution in PBS (2 mg/kg body weight, twice a week), and mice in the control group were i.p. injected with the same volume of PBS. At the end of experiment, mice were anesthetized and euthanized in a CO_2 chamber, followed by collection of blood, aorta, and liver samples.

Collection of aortas and determination of atherosclerotic lesions

To determine aortic lesions, aorta samples were collected from mice after euthanasia as described (17). After removing the outside connecting tissue and fat, the aortas were stained with Oil Red O working solution (3 mg/ml in 60% isopropyl alcohol) for 40 min and then rinsed with 60% isopropyl alcohol three times. Finally, aortas were rinsed twice with distilled water. Images of aortas were obtained with a Leica microscope (Wetzlar, Germany). The lesion areas of *en face* aorta, aortic arch, descending aorta, thoracic aorta, and abdominal aorta were quantitatively determined with a computer-assisted image analysis method (Photoshop CS3) and presented as μm^2.

To determine the sinus lesions in aortic root, Oil Red O staining was conducted on the 5-μm frozen sections of aortic root. Similarly, the lesion areas were quantified using Photoshop CS3 and expressed as μm^2.

H&E, VVG, and immunofluorescent staining

To determine and quantify the area of necrotic cores, thickness of fibrosis cap, collagen content, and expression of αSMA, OPN, MOMA2, ABCA1, ABCG1, RUNX2, ALP, and MMP9 in lesion areas, H&E, VVG, and immunofluorescent staining were performed on aortic root cross-sections, respectively (17). After staining, sections were mounted with resinous mounting medium. Images were captured by a Leica microscope.

Cell culture

HASMCs were purchased from ATCC (Manassas, VA, USA), and cultured in DMEM/F-12 (1:1) medium containing 10% fetal bovine serum, 50 μg/ml penicillin/streptomycin, and 2 mM glutamine. Cells at ~90% confluence were switched into serum-free medium before the indicated treatment. Peritoneal macrophages were collected from mouse as described (20). Cells were cultured in complete RPMI 1640 medium containing 10% fetal bovine serum, 50 μg/ml penicillin/streptomycin, and 2 mM glutamine for 2 days before the indicated treatment.

Western blotting and quantitative real-time PCR (qRT-PCR)

After treatment, total cellular and nuclear proteins were extracted from cells (17). Expression of proteins in macrophages or HASMCs was determined by Western blotting.

TRIzol reagent was used to extract total RNA from HASMCs or liver samples, and mRNA expression was determined by qRT-PCR with a reverse transcription kit (New England Biolabs, Ipswich, MA, USA), SYBR Green PCR master mix (Vazyme, Nanjing, China), and the primers listed in Table 2 or Table S1. Relative mRNA levels were normalized by GAPDH mRNA in the corresponding samples. The miRNA expression in HASMCs was analyzed by quantitative miR stem-loop RT-PCR technology (Ambion) (37).

Determination of foam cell formation by Oil Red O staining

In vitro, we utilized Oil Red O staining to evaluate formation of foam cells. First, cells were plated on coverslips in 48-well plates and cultured to ~70% confluence. Cells were then treated with TL1A, oxLDL (50 μg/ml), or TL1A plus oxLDL for the indicated time in serum-free medium. After treatment, cells were fixed with 4% paraformaldehyde for 30 min at room temperature after gently washing with PBS. Cells were then stained with Oil Red O and hematoxylin. The slides were observed under a Leica DM3000 microscope (Wetzlar, Germany) with images photographed. Foam cells (>10 lipid droplets/cell) were counted with ~6 fields/sample (17).

Determination of cholesterol efflux to HDL

The cholesterol efflux was determined as described (39). Briefly, cells at ~90% confluence in 24-well plates were radiolabeled in serum-free medium containing 50 μg/ml acetylated LDL and 150 nCi/ml [^{3}H]cholesterol for 24 h, washed with PBS twice, and then treated with TL1A for 24 h. After incubation with serum-free medium containing HDL (15 μg/ml) for 6 h, medium was collected and centrifuged at 900 × *g* for 2 min to remove detached cells, followed by determination of radioactivity in the medium with a liquid scintillation. Cells were lysed, and cellular protein was determined, which was used to normalize cholesterol efflux. The data were expressed as fold of control.

Determination of vascular calcification in aortas and HASMCs

To induce vascular calcification *in vitro*, HASMCs at ~90% confluence in 24-well plates were cultured in complete

Figure 5. TL1A inhibits VSMC calcification by regulating RUNX2 pathway. *A* and *B*, aortic cross-sections were subjected to immunofluorescent staining with anti-RUNX2, ALP, or MMP9 antibody, and MFI in images was quantitatively analyzed. *Scale bar* in *insets*, 25 μm. The *NC* was conducted with an adjacent slide to the *NC* slide in the *right panel* of Fig. 3*A* (for OPN). *, $p < 0.05$; **, $p < 0.01$ ($n = 6$). *C–J*, HASMCs were cultured in complete DMEM/F-12 medium (*control*) or calcification medium (complete DMEM/F-12 medium was added with 10 mM β-glycerophosphate disodium salt and 250 μM ascorbic acid; *vehicle/CM*) or plus TL1A (200 ng/ml) for 2 weeks. Calcium deposition in cells was determined by Alizarin Red S staining (*C*). Cellular calcium content was quantified using the calcium assay kit (*D*). Expression of RUNX2 protein in HASMCs was determined by immunofluorescence staining with quantitation of MFI (*E*). *, $p < 0.05$; *NS*, not significantly different ($n = 6$). Expression of RUNX2 protein in total cellular and nuclear extract (*F* and *G*) and BMP2, ALP, and OPN in total cellular extract (*H* and *I*) was determined by Western blotting with quantitative analysis of band density. Expression of BMP2, ALP, and OPN mRNA was determined by qRT-PCR (*J*). *, $p < 0.05$; *NS*, not significantly different ($n = 3$). *K* and *L*, ~90% confluent HASMCs in serum-free medium were transfected with the plasmid DNA for empty vector or RUNX2 promoter and *Renilla* (as an internal control) for 24 h, followed by TL1A (200 ng/ml) treatment in serum-free normal medium or serum-free calcification medium (*CM*) for 24 h (*K*), or ~90% confluent HASMCs in 48-well plates were precultured in serum-free normal medium or serum-free calcification medium for 24 h and then transfected with the indicated DNA for 24 h in serum-free medium, followed by 24-h TL1A (200 ng/ml) treatment in the indicated medium (*L*). Total cellular lysate was extracted and used to determine firefly and *Renilla* luciferase (*luc*) activity. *, $p < 0.05$; *NS*, not significantly different ($n = 5$). *Error bars*, S.D.

Table 2
Sequences of the primers for qRT-PCR analysis. h and Has, *Homo sapiens*

Gene	Forward	Reverse
hαSMA	GCGTGGCTATTCCTTCGTTA	ATGAAGGATGGCTGGAACAG
hSM22α	AACAGCCTGTACCCTGATGG	CGGTAGTGCCCATCATTCTT
hOPN	AATTGCAGTGATTTGCTTTTGC	CAGAACTTCCAGAATCAGCCTGTT
hEREG	TCACTGCGACATGATTAATGGTAC	ACGTCGGATTCAAATACAGCATAGAT
hSRF	CCTGAATCGAGCTGAGAGGG	TGTGATGCTGCTCAGGTGTG
hMyocd	GCAAAGATTCCACTTTGCGT	GAAATTGCAGGAGGAGATGC
hMsx1	TTGCCACTCGGTGTCAAAGT	AAGGGGACACTTTGGGCTTG
hMsx2	CTGGTGAAGCCCTTCGAGAC	ATATGTCCTCCTACTCCTGCCC
hRUNX2	GCAAGGTTCAACGATCTGAGATT	AAGACGGTTATGGTCAAGGTGAAA
hALP	ACCACCACGAGAGTGAACCA	CGTTGTCTGAGTACCAGTCCC
hBMP2	AGGAGGCAAAGAAAAGGAACGGAC	GGAAGCAGCAACGCTAGAAGACAG
hGAPDH	TGATGACATCAAGAAGGTGGTGAAG	TCCTTGGAGGCCATGTGGGCCAT
Has-miR214-5p	GTGCAGGGTCCGAGGT	GCCGCTGCCTGTCTACACTTG
Has-miR145	GTGCAGGGTCCGAGGT	GTCCAGTTTTCCCAGGAATCC
Has-miR203-3p	GTGCAGGGTCCGAGGT	TAGCGTGAAATGTTTAGGACC
Has-miR29-5p	GTGCAGGGTCCGAGGT	GCCGCGCTGGTTTCATATGGTGG
U6	CTCGCTTCGGCAGCACA	AACGCTTCACGAATTTGCGT

DMEM/F-12 medium or the medium supplemented with 10 mM β-glycerophosphate disodium salt and 250 μM ascorbic acid (this medium was named calcification medium) to induce calcification for 2 weeks. During the process of calcification, the medium was changed once every other day (37).

Calcium deposit in cells or aortic sections was determined by Alizarin Red S staining, followed by photograph with an optical microscope. The positively stained calcification area in aortas displays a red-orange color and was quantified using ImageJ software (National Institutes of Health).

Calcium content in HASMCs was quantitatively analyzed by the Calcium LiquiColor kit (Biovision, Inc., Milpitas, CA) as described (37). Calcium levels were normalized by protein concentration in the corresponding samples, and the data were expressed as μg/mg protein.

Inhibition of p53 expression by siRNA

The siRNAs against human p53 and scrambled siRNA were purchased from Santa Cruz Biotechnology, Inc. (Dallas, TX, USA). HASMCs were transfected with siRNA using Lipofectamine RNAiMAX Transfection Reagent (Invitrogen). After 24 h of transfection, cells were switched to complete DMEM/F-12 (1:1) medium for another 24 h, followed by determination of protein expression by Western blotting (37).

Determination of RUNX2 promoter activity

The human RUNX2 promoter (*p*RUNX2, from −1817 to +101) was constructed by PCR with human genomic DNA and the following primers: forward, 5′-CGGGGTACCAAATGAACGCTTTTACCT-3′; reverse, 5′-CCGCTCGAGTAGTGACCTGCGGAGATT-3′. After the sequence was confirmed, the PCR product was digested with XhoI and KpnI, followed by ligation into the pGL4 luciferase reporter vector and then transformed into *Escherichia coli* for amplification.

To analyze RUNX2 promoter activity in the calcified conditions, ~90% confluent HASMCs in 48-well plates were cultured in serum-free medium or calcification medium for 24 h and then transfected with plasmid DNA for the RUNX2 promoter and *Renilla* (for internal normalization) for 24 h, followed by 24-h TL1A treatment. Cells were lysed, and the cellular lysate was used to determine the activity of firefly and *Renilla* luciferases using the Dual-Luciferase reporter assay system (Promega, Madison, WI) (20).

Determination of serum biochemical parameters

After collection, blood samples were kept for 2 h at room temperature, followed by centrifugation for 20 min at 2,000 × *g* at room temperature. Serum was transferred into a new test tube and used to determine levels of triglyceride, total, LDL- and HDL-cholesterol, AST, ALT, and ALP using an automatic biochemical analyzer (model 7020; Hitachi, Tokyo, Japan).

Statistical analysis

All experiments were repeated at least three times, and the representative results are presented. For Western blotting assays, the target bands were normalized to GAPDH in the corresponding sample to reduce variance. The staining was completed with more than three sections from each group. The statistical results in all figures and tables are presented as mean ± S.D. All of the data in normal distribution were then analyzed by unpaired Student's *t* test or post hoc test of one- or two-way analysis of variance after evaluation of variance homogeneity ($n \geq 3$). The differences were considered significant at $p < 0.05$.

Data availability

All the data related to this work are included in the article or supporting information.

Acknowledgment—Dan Zhao received the American Society of Biochemistry and Molecular Biology Graduate/Postdoctoral Travel Award and an invitation to orally present this work at "Experimental Biology 2019" in Orlando, Florida, April 2019.

Author contributions—D. Z., J. L., C. X., K. F., L. Liu, P. Z., X. W., and Y. C. data curation; D. Z., J. L., K. F., L. Liu, and Y. C. formal analysis; D. Z., C. X., and Z. Z. methodology; L. Li and Z. Z. resources; L. Li software; Y. D., J. H., and X. Y. funding acquisition; Y. D. and X. Y. writing-original draft; Y. D. project administration; J. H.

and X. Y. conceptualization; J. H. and X. Y. supervision; J. H. visualization; J. H. writing-review and editing.

Funding and additional information—This work was supported by the International Science and Technology Cooperation Programs of China Grant 2017YFE0110100 to (J. H., Y. D., X. Y., and Y. C.); National Natural Science Foundation of China (NSFC) Grants 81803517 (to X. Y.), 81773727 and 81973316 (to J. H.), 81722046 (to Y. D.), and 31770863 (to Y. C.); Key Research and Development Program of Anhui Province Grant 201904a07020007 (to J. H.); and the Fundamental Research Funds for the Central Universities (to X. Y., Y. D., and Y. C.).

Conflict of interest—The authors declare that they have no conflicts of interest with the contents of this article.

Abbreviations—The abbreviations used are: VSMC, vascular smooth muscle cell; apoE$^{-/-}$, apoE-deficient; ABCA1, ATP-binding cassette transporter A1; ABCG1, ATP-binding cassette transporter G1; ATGL, adipose triglyceride lipase; AST, aspartate aminotransferase; ALT, alanine aminotransferase; ALP, alkaline phosphatase; αSMA, α smooth muscle actin; BMP2, bone morphogenetic protein 2; DGAT1, acyl-CoA:diacylglycerol acyltransferase 1; EREG, epiregulin; HASMC, human aortic smooth muscle cell; H&E, hematoxylin and eosin; LDL, low-density lipoprotein; HDL, high-density lipoprotein; HFD, high-fat diet; HSL, hormone-sensitive lipase; LXR, liver X receptor; MFI, mean fluorescent intensity; miRNA, microRNA; MMP, matrix metallopeptidase; MOMA2, monocyte/macrophage marker 2; Msx1, Msh homeobox 1; Msx2, Msh homeobox 2; Myocd, myocardin; NC, negative control; oxLDL, oxidized low-density lipoprotein; OPN, osteopontin; PPAR, peroxisome proliferator-activated receptor; qRT-PCR, quantitative real-time PCR; RUNX2, runt-related transcription factor 2; SM22α, smooth muscle protein 22α; SRF, serum response factor; TL1A, TNF ligand-related molecule 1A; VVG, Verhoeff–Van Gieson; TUNEL terminal deoxynucleotidyl transferase dUTP-mediated nick-end labeling; i.p., intraperitoneally; DMEM, Dulbecco's modified Eagle's medium; GAPDH, glyceraldehyde-3-phosphate dehydrogenase.

References

1. Wolf, D., and Ley, K. (2019) Immunity and inflammation in atherosclerosis. *Circ. Res.* **124,** 315–327 CrossRef Medline
2. Weber, C., and Noels, H. (2011) Atherosclerosis: current pathogenesis and therapeutic options. *Nat. Med.* **17,** 1410–1422 CrossRef Medline
3. Gimbrone, M. A., Jr., and García-Cardeña, G. (2016) Endothelial cell dysfunction and the pathobiology of atherosclerosis. *Circ. Res.* **118,** 620–636 CrossRef Medline
4. Bennett, M. R., Sinha, S., and Owens, G. K. (2016) Vascular smooth muscle cells in atherosclerosis. *Circ. Res.* **118,** 692–702 CrossRef Medline
5. Li, P., Zhu, N., Yi, B., Wang, N., Chen, M., You, X., Zhao, X., Solomides, C. C., Qin, Y., and Sun, J. (2013) MicroRNA-663 regulates human vascular smooth muscle cell phenotypic switch and vascular neointimal formation. *Circ. Res.* **113,** 1117–1127 CrossRef Medline
6. Yurdagul, A., Jr., Finney, A. C., Woolard, M. D., and Orr, A. W. (2016) The arterial microenvironment: the where and why of atherosclerosis. *Biochem. J.* **473,** 1281–1295 CrossRef Medline
7. Gomez, D., and Owens, G. K. (2012) Smooth muscle cell phenotypic switching in atherosclerosis. *Cardiovasc. Res.* **95,** 156–164 CrossRef Medline
8. Durham, A. L., Speer, M. Y., Scatena, M., Giachelli, C. M., and Shanahan, C. M. (2018) Role of smooth muscle cells in vascular calcification: implications in atherosclerosis and arterial stiffness. *Cardiovasc. Res.* **114,** 590–600 CrossRef Medline
9. Chaabane, C., Coen, M., and Bochaton-Piallat, M. L. (2014) Smooth muscle cell phenotypic switch: implications for foam cell formation. *Curr. Opin. Lipidol.* **25,** 374–379 CrossRef Medline
10. Allahverdian, S., Chehroudi, A. C., McManus, B. M., Abraham, T., and Francis, G. A. (2014) Contribution of intimal smooth muscle cells to cholesterol accumulation and macrophage-like cells in human atherosclerosis. *Circulation* **129,** 1551–1559 CrossRef Medline
11. Wang, Y., Dubland, J. A., Allahverdian, S., Asonye, E., Sahin, B., Jaw, J. E., Sin, D. D., Seidman, M. A., Leeper, N. J., and Francis, G. A. (2019) Smooth muscle cells contribute the majority of foam cells in apoE (apolipoprotein E)-deficient mouse atherosclerosis. *Arterioscler. Thromb. Vasc. Biol.* **39,** 876–887 CrossRef Medline
12. Rudijanto, A. (2007) The role of vascular smooth muscle cells on the pathogenesis of atherosclerosis. *Acta Med. Indones.* **39,** 86–93 Medline
13. Bayry, J. (2010) Immunology: TL1A in the inflammatory network in autoimmune diseases. *Nat. Rev. Rheumatol.* **6,** 67–68 CrossRef Medline
14. Zhang, K., Cai, H. X., Gao, S., Yang, G. L., Deng, H. T., Xu, G. C., Han, J., Zhang, Q. Z., and Li, L. Y. (2016) TNFSF15 suppresses VEGF production in endothelial cells by stimulating miR-29b expression via activation of JNK-GATA3 signals. *Oncotarget* **7,** 69436–69449 CrossRef Medline
15. Kang, Y. J., Kim, W. J., Bae, H. U., Kim, D. I., Park, Y. B., Park, J. E., Kwon, B. S., and Lee, W. H. (2005) Involvement of TL1A and DR3 in induction of pro-inflammatory cytokines and matrix metalloproteinase-9 in atherogenesis. *Cytokine.* **29,** 229–235 CrossRef Medline
16. McLaren, J. E., Calder, C. J., McSharry, B. P., Sexton, K., Salter, R. C., Singh, N. N., Wilkinson, G. W., Wang, E. C., and Ramji, D. P. (2010) The TNF-like protein 1A-death receptor 3 pathway promotes macrophage foam cell formation *in vitro*. *J. Immunol.* **184,** 5827–5834 CrossRef Medline
17. Ma, C., Zhang, W., Yang, X., Liu, Y., Liu, L., Feng, K., Zhang, X., Yang, S., Sun, L., Yu, M., Yang, J., Li, X., Hu, W., Miao, R. Q., Zhu, Y., *et al.* (2018) Functional interplay between liver X receptor and AMP-activated protein kinase α inhibits atherosclerosis in apolipoprotein E-deficient mice-A new anti-atherogenic strategy. *Br. J. Pharmacol.* **175,** 1486–1503 CrossRef Medline
18. Nakashima, Y., Plump, A. S., Raines, E. W., Breslow, J. L., and Ross, R. (1994) ApoE-deficient mice develop lesions of all phases of atherosclerosis throughout the arterial tree. *Arterioscler. Thromb.* **14,** 133–140 CrossRef Medline
19. Finn, A. V., Nakano, M., Narula, J., Kolodgie, F. D., and Virmani, R. (2010) Concept of vulnerable/unstable plaque. *Arterioscler. Thromb. Vasc. Biol.* **30,** 1282–1292 CrossRef Medline
20. Yang, X., Zhang, W., Chen, Y., Li, Y., Sun, L., Liu, Y., Liu, M., Yu, M., Li, X., Han, J., and Duan, Y. (2016) Activation of peroxisome proliferator-activated receptor gamma (PPARγ) and CD36 protein expression: the dual pathophysiological roles of progesterone. *J. Biol. Chem.* **291,** 15108–15118 CrossRef Medline
21. Zhao, C., and Dahlman-Wright, K. (2010) Liver X receptor in cholesterol metabolism. *J. Endocrinol.* **204,** 233–240 CrossRef Medline
22. Han, H., Yang, S., Liang, Y., Zeng, P., Liu, L., Yang, X., Duan, Y., Han, J., and Chen, Y. (2018) Teniposide regulates the phenotype switching of vascular smooth muscle cells in a miR-21-dependent manner. *Biochem. Biophys. Res. Commun.* **506,** 1040–1046 CrossRef Medline
23. Sahoo, S., Meijles, D. N., Al Ghouleh, I., Tandon, M., Cifuentes-Pagano, E., Sembrat, J., Rojas, M., Goncharova, E., and Pagano, P. J. (2016) MEF2C-MYOCD and leiomodin1 suppression by miRNA-214 promotes smooth muscle cell phenotype switching in pulmonary arterial hypertension. *PLoS ONE* **11,** e0153780 CrossRef Medline
24. Cordes, K. R., Sheehy, N. T., White, M. P., Berry, E. C., Morton, S. U., Muth, A. N., Lee, T. H., Miano, J. M., Ivey, K. N., and Srivastava, D. (2009) miR-145 and miR-143 regulate smooth muscle cell fate and plasticity. *Nature* **460,** 705–710 CrossRef Medline
25. Shen, L., Song, Y., Fu, Y., and Li, P. (2018) MiR-29b mimics promotes cell apoptosis of smooth muscle cells via targeting on MMP-2. *Cytotechnology* **70,** 351–359 CrossRef

26. Zhang, J. R., Lu, Q. B., Feng, W. B., Wang, H. P., Tang, Z. H., Cheng, H., Du, Q., Wang, Y. B., Li, K. X., and Sun, H. J. (2018) Nesfatin-1 promotes VSMC migration and neointimal hyperplasia by upregulating matrix metalloproteinases and downregulating PPARγ. *Biomed. Pharmacother.* **102,** 711–717 CrossRef Medline
27. Tan, Z., Li, J., Zhang, X., Yang, X., Zhang, Z., Yin, K. J., and Huang, H. (2018) p53 promotes retinoid acid-induced smooth muscle cell differentiation by targeting myocardin. *Stem Cells Dev.* **27,** 534–544 CrossRef Medline
28. Shioi, A., and Ikari, Y. (2018) Plaque calcification during atherosclerosis progression and regression. *J. Atheroscler. Thromb.* **25,** 294–303 CrossRef Medline
29. Leopold, J. A. (2015) Vascular calcification: mechanisms of vascular smooth muscle cell calcification. *Trends Cardiovasc. Med.* **25,** 267–274 CrossRef Medline
30. Tu, B., Liu, S., Yu, B., Zhu, J., Ruan, H., Tang, T., and Fan, C. (2016) miR-203 inhibits the traumatic heterotopic ossification by targeting Runx2. *Cell Death Dis.* **7,** e2436 CrossRef Medline
31. Hsu, H., and Viney, J. L. (2011) The tale of TL1A in inflammation. *Mucosal Immunol.* **4,** 368–370 CrossRef Medline
32. Chen, Y., Duan, Y., Yang, X., Sun, L., Liu, M., Wang, Q., Ma, X., Zhang, W., Li, X., Hu, W., Miao, R. Q., Xiang, R., Hajjar, D. P., and Han, J. (2015) Inhibition of ERK1/2 and activation of LXR synergistically reduce atherosclerotic lesions in ApoE-deficient mice. *Arterioscler. Thromb. Vasc. Biol.* **35,** 948–959 CrossRef Medline
33. Ma, J., Zhao, D., Wang, X., Ma, C., Feng, K., Zhang, S., Chen, Y., Zhu, Y., Gao, X., Zhao, B., Wang, Y., Qian, K., Li, X., Duan, Y., Han, J., *et al.* (2019) LongShengZhi capsule reduces established atherosclerotic lesions in apoE-deficient mice by ameliorating hepatic lipid metabolism and inhibiting inflammation. *J. Cardiovasc. Pharmacol.* **73,** 105–117 CrossRef Medline
34. Quiroga, A. D., and Lehner, R. (2012) Liver triacylglycerol lipases. *Biochim. Biophys. Acta* **1821,** 762–769 CrossRef Medline
35. Allahverdian, S., Chaabane, C., Boukais, K., Francis, G. A., and Bochaton-Piallat, M. L. (2018) Smooth muscle cell fate and plasticity in atherosclerosis. *Cardiovasc. Res.* **114,** 540–550 CrossRef Medline
36. Guevara, N. V., Kim, H. S., Antonova, E. I., and Chan, L. (1999) The absence of p53 accelerates atherosclerosis by increasing cell proliferation *in vivo*. *Nat. Med.* **5,** 335–339 CrossRef Medline
37. Liu, L., Zeng, P., Yang, X., Duan, Y., Zhang, W., Ma, C., Zhang, X., Yang, S., Li, X., Yang, J., Liang, Y., Han, H., Zhu, Y., Han, J., and Chen, Y. (2018) Inhibition of vascular calcification. *Arterioscler. Thromb. Vasc. Biol.* **38,** 2382–2395 CrossRef Medline
38. Allahverdian, S., Pannu, P. S., and Francis, G. A. (2012) Contribution of monocyte-derived macrophages and smooth muscle cells to arterial foam cell formation. *Cardiovasc. Res.* **95,** 165–172 CrossRef Medline
39. Zhang, L., Chen, Y., Yang, X., Yang, J., Cao, X., Li, X., Li, L., Miao, Q. R., Hajjar, D. P., Duan, Y., and Han, J. (2016) MEK1/2 inhibitors activate macrophage ABCG1 expression and reverse cholesterol transport: an antiatherogenic function of ERK1/2 inhibition. *Biochim. Biophys. Acta* **1861,** 1180–1191 CrossRef Medline
40. Schroeder, F., Huang, H., Hostetler, H. A., Petrescu, A. D., Hertz, R., Bar-Tana, J., and Kier, A. B. (2005) Stability of fatty acyl-coenzyme A thioester ligands of hepatocyte nuclear factor-4α and peroxisome proliferator-activated receptor-α. *Lipids* **40,** 559–568 CrossRef Medline
41. Sun, L., Yang, X., Li, Q., Zeng, P., Liu, Y., Liu, L., Chen, Y., Yu, M., Ma, C., Li, X., Li, Y., Zhang, R., Zhu, Y., Miao, Q. R., Han, J., and Duan, Y. (2017) Activation of adiponectin receptor regulates proprotein convertase subtilisin/kexin type 9 expression and inhibits lesions in apoE-deficient mice. *Arterioscler. Thromb. Vasc. Biol.* **37,** 1290–1300 CrossRef Medline